Ultrasound validation of mathematically modeled irreversible electroporation ablation areas

Neal Bhutiani, MD, Cathryn A. Doughtie, MD, *and* **Robert C. G. Martin II, MD, PhD, FACS,**
Louisville, KY

Objective. *Currently, the prediction of the dimensions of irreversible electroporation (IRE) ablation is modeled using algorithms derived from mathematical and ex vivo models. These algorithms have not been validated using in vivo studies. The aim of this study was to assess the correlation between the mathematical prediction model to and ultrasonographic and histopathologic findings for in vivo ablations in a porcine model.*

Methods. *IRE ablations were performed on porcine liver and spleen with probe spacings ranging from 0.6 to 2.6 cm. Pre and 2-hour postablation ultrasound (US) images were recorded and validated with confirmation by histopathology. Three dimensions of the regions of ablation were recorded, and ablation volumes were calculated and correlated with theoretic mathematical models for each given probe spacing.*

Results. *In vivo axial and anterior-posterior (AP) distances of ablation were greater than predicted for nearly all probe spacings ($P < .05$). Ablation volumes were significantly less than predicted for the all probe spacings when modeled using both a cylinder and an ellipsoid. Geometrically, mathematically derived regions of ablation demonstrated more central tapering ("necking") and diminished volumes compared to their in vivo counterparts. The relationships between probe spacing and AP dimensions of ablation were less linear ($r^2 = 0.57$) than the relationships observed via ultrasonography.*

Conclusion. *The current mathematical models predict regions of ablation observed in vivo poorly. They underestimate dimensions of ablation and, by extension, the volumes of ablation. Further work should be done to improve models for ablative planning, and physicians should recognize the limitations of existing models when planning ablative treatments. (Surgery 2016;159:1032-40.)*

From the Hiram C. Polk Jr, MD Department of Surgery, University of Louisville, Louisville, KY

Currently, multiple methods of thermal ablation are used to treat locally a variety of malignancies of the liver, lung, and kidney. Irreversible electroporation (IRE) has emerged as a non-thermal alternative, and thus has a theoretic advantage over radiofrequency/microwave/cyroablation/high-frequency ultrasound ablation by being able to treat a similar volume of tissue with minimal damage to surrounding tissues.[1-9] Since that time, various studies have demonstrated the safety and efficacy of IRE in a number of different settings, with the most promising results in locally advanced pancreatic cancer, hepatocellular carcinoma, liver metastases from various sources, and prostate cancer.[1,2,4-8,10-14] Currently, hepatic and pancreatic lesions represent those neoplasms targeted most frequently with IRE owing to the greatest demonstrated efficacy in treating neoplasms in these 2 organs.

For each of these malignancies, standardized protocols have been developed regarding voltage across electrodes as well as number and duration of pulses. Lesions are identified routinely, and electrode placement is performed by bracketing the target lesion using intraoperative ultrasonography or computed tomography (CT) guidance. Electrode placement is determined based on the desired region of ablation. These regions to be ablated have been calculated using mathematical models developed by AngioDynamics.[15] Given the heterogeneity of tissues, this model uses a test pulse between probes after placement to account for variables, such as tissue conductivity, resistivity, and density. It is important to note that IRE works by inducing pores in the cellular phospholipid bilayer via an electric current. Like other ablative

Accepted for publication October 28, 2015.

Reprint requests: Robert C. G. Martin II, MD, PhD, FACS, Professor of Surgery, Director, Division of Surgical Oncology, Director, Upper Gastrointestinal and Hepato-Pancreatico-Biliary Clinic Academic Advisory Dean, 315 E. Broadway #311, Louisville, KY 40202. E-mail: Robert.Martin@louisville.edu.

0039-6060/$ - see front matter

http://dx.doi.org/10.1016/j.surg.2015.10.030

modalities, IRE is influenced by tissue density, conductivity, and water content like other ablative modalities, but importantly IRE is not influenced by the heat sink effect. Furthermore, whereas other ablative modalities induce cell death via necrosis, IRE induces apoptotic cell death.

Studies have examined postablation histologic and ultrasonographic findings both immediately postablation and over time showing correlation between cell death via apoptosis and change in tissue characteristics.[1,16] Further investigations have imaged the areas of ablation using MRI as well as CT and have characterized postablation changes using these modalities.[1,17,18] Investigators have correlated histopathology with modeled predictions of ablation as well as preablation and postablation imaging characteristics on CT.[17,19-21] These studies have suggested that peripheral apoptotic effects are less permissive than those closer to the electrodes and that models may underestimate the actual volume of tissue effected by a given electroporation treatment.

Despite the extensive analysis of ablation zones via histopathology as well as various imaging modalities, no studies have used in vivo ultrasonography and histopathologic confirmation to validate the regions of ablation calculated via mathematical algorithm that determines electrode spacing intraprocedurally. In this study, we aim to validate the mathematical modeling predicted electroporation volume with in vivo histopathologic findings. In doing so, we assessed the accuracy of preexisting mathematical models of ablation.

METHODS AND MATERIALS

Animals. This study was conducted in accordance with the National Institutes of Health guidelines for the care and use of animals in research, and the protocol was approved by the Animal Care and Use Committee of the University of Louisville. The University of Louisville animal care and use program is fully accredited by the American Association for the Accreditation of Laboratory Animal Care, International. Five female, all-white Yorkshire × Landrace swine (*Sus scrofa*) from Oak Hill Genetics (Ewing, IL) were obtained at 8–10 months of age, weighing 85–90 kg at the time of arrival. During quarantine and acclimation, animals were group housed in pens with elevated fiberglass slatted floors providing a minimum 20 ft^2 per animal in a temperature (22.0–22.0°C) and humidity (30–70%) controlled room on a 12:12 hour light:dark cycle. Pens were cleaned daily, and animals were fed 5084 Laboratory Porcine Diet Grower (LabDiet, PMI Nutrition International, Richmond, IN) twice daily in amounts recommended by the manufacturer. Animals were provided filtered tap water ad libidum from arrival through the end of the study. Animals were free of the following pathogens: *Actinobacacillus pleuropneumoniae*, *Mycoplasma pneumonia*, porcine reproductive and respiratory syndrome, atrophic rhinitis, Pneudorabies virus, and acute malignant hypothermia. Animals were free of internal and external parasites. Before any experimental manipulations were initiated, animals were allowed to acclimate for ≥7 days. Veterinary staff assessed the animals before each procedure for general health, vital signs, oral intake, and urine and fecal output. Baseline complete blood cell counts and serum biochemistries were performed before operation.

Technique of ablation. Transdermal fentanyl patches (50 μg/h, Ortho-McNeil-Janssen Pharmaceuticals Inc., Raritan, NJ) were applied onto the skin of the shoulders of the animals the evening before operation. The animals were fasted for 12 hours, but access to water was not restricted. The animals were anesthetized with subcutaneous 4.4 mg/kg telazol (Fort Dodge Animal Health, Overland Park, KS), 2.2 mg/kg ketamine (Fort Dodge Animal Health), and 2.2 mg/kg xylazine (Butler Animal Health, Dublin, OH). The animals were then intubated and maintained on 1–3% Isoflurane (Butler Animal Health) and 100% oxygen. Artificial Tears ophthalmic ointment (Butler Animal Health), was applied to the surface of both eyes. Body temperature was maintained with a warm air circulating blanket (Bair Hugger, Arizant Healthcare, Eden Prairie, MN). A 20-gauge intravenous catheter was placed in the marginal ear vein, and 10 mL/kg/h Normosol-R (Hospira, Lake Forest, IL) was administered to maintain blood pressure. Each animal received 2 mg/kg carprofen IV (Pfizer Animal Health, New York, NY) and 0.04 mg/kg buprenorphine IV (Butler Animal Health) for analgesia before operation. The animals were placed on mechanical ventilation, and heart rate, body temperature, SpO_2, reflexes, and blood pressure were monitored continuously throughout the anesthetic procedure to maintain the animals in a surgical plane of anesthesia. To control muscle twitches during IRE, 30 mg succinylcholine (Butler Animal Health) was administered intravenously and was readministered as needed during the procedure based on muscle twitches of the animal. Each animal was placed in dorsal recumbency. A 7-French polysulfone vascular access port (Access Technologies, Skokie,

Table I. Expected ablation dimensions

Probe spacing (cm)	*Expected axial (cm)*	*Expected AP ablation (cm)*	*Expected craniocaudal (cm)*	*Expected ablation volume (cm^3)*	*Expected ablation volume – ellipsoid (cm^3)*
0.6	0.2	0.2	0.8	0.0063	0.0168
0.8	0.8	0.4	1.0	0.1005	0.1676
1.0	1.4	0.3	1.6	0.0990	0.3519
1.0	1.4	0.3	1.4	0.0990	0.3079
1.2	1.8	0.9	1.6	1.1451	1.3572
1.2	1.8	0.9	1.6	1.1451	1.3572
1.4	2.3	1.1	1.7	2.1858	2.2520
1.4	2.3	1.1	1.7	2.1858	2.2520
1.6	2.7	1.4	1.9	4.1563	3.7605
1.6	2.7	1.4	1.9	4.1563	3.7605
1.8	2.9	1.5	1.9	5.1247	4.3275
1.8	2.9	1.5	1.9	5.1247	4.3275
2.0	3.2	1.6	2.0	6.4340	5.3616
2.0	3.2	1.6	2.0	6.4340	5.3616
2.2	3.3	1.4	2.0	5.0800	4.8380
2.2	3.3	1.4	2.0	5.0800	4.8380
2.4	3.4	1.2	1.9	3.8453	4.0589
2.4	3.4	1.2	1.9	3.8453	4.0589
2.6	3.6	1.1	1.7	3.4212	3.5249
2.6	3.6	1.1	1.7	3.4212	3.5249

IL) was implanted in the external jugular vein for refinement of blood collection, as well as administration of drugs and fluids postoperatively. The vascular access ports were exteriorized on the dorsal neck owing to the relatively short duration of the study and to minimize potential pain and distress to the animals of repeated daily access. Access to the liver and spleen was made through a ventral midline incision.

Ablations were performed using 19-gauge monopolar electrodes. The electrodes were placed within the liver or spleen using continuous ultrasound (US) guidance. Monopolar electrodes were spaced at varying intervals of between 0.6 and 2.6 cm using an attached spacing device per the manufacturer's modeling algorithm. Probe spacing was confirmed using US. The depth of exposed electrode was also varied depending on the vascular anatomy and size of the liver and spleen available.

Expected dimensions of ablation were generated using a proprietary algorithm developed by AngioDynamics using exposure time and probe spacing.[15] Briefly, this algorithm takes into account water content of tissue, tissue density, tissue type, conductivity, and resistivity. The patient[15] defines extensively the methods that the original and current systems use. The current IRE system is not a dynamic system; it does not have the ability to modify the energy delivered based on these multiple changes. A test pulse between probes was used to evaluate tissue-specific variables, including tissue conductivity and resistivity. Visual representations of the regions of ablation were generated along with expected axial and anterior-posterior (AP) parameters/distances of ablation. The expected volume of ablation was calculated as the volume of a cylinder using expected axial and AP ablations.

The IRE current generator (NanoKnife; AngioDynamics: Queensbury, NY, Energy output – 3 kV, 50-amp maximum energy output) was synchronized to deliver electrical pulses coordinated with the cardiac rhythm of each pig to prevent cardiac dysrhythmias. Each ablation began with a test pulse at 10% planned energy output to assess that an adequate current was achieved. After successful test pulse, the therapeutic pulses were then delivered. As reported previously in prior animal models, the goal of treatment was to deliver 90 electrical microsecond pulses in groups of 10 with a pulse duration of 100 μsec and a pulse interval of 250 msec. These parameters were chosen as a conservative estimate of the electrical field needed to induce IRE in a hepatic tumor. Ablation sizes were measured using US as longest length (ie, along the probe), longest width, and greatest depth. Volumes of ablation were calculated as the volume of an ellipsoid using these parameters. All dimensions of ablation as measured by US were validated histopathologically.

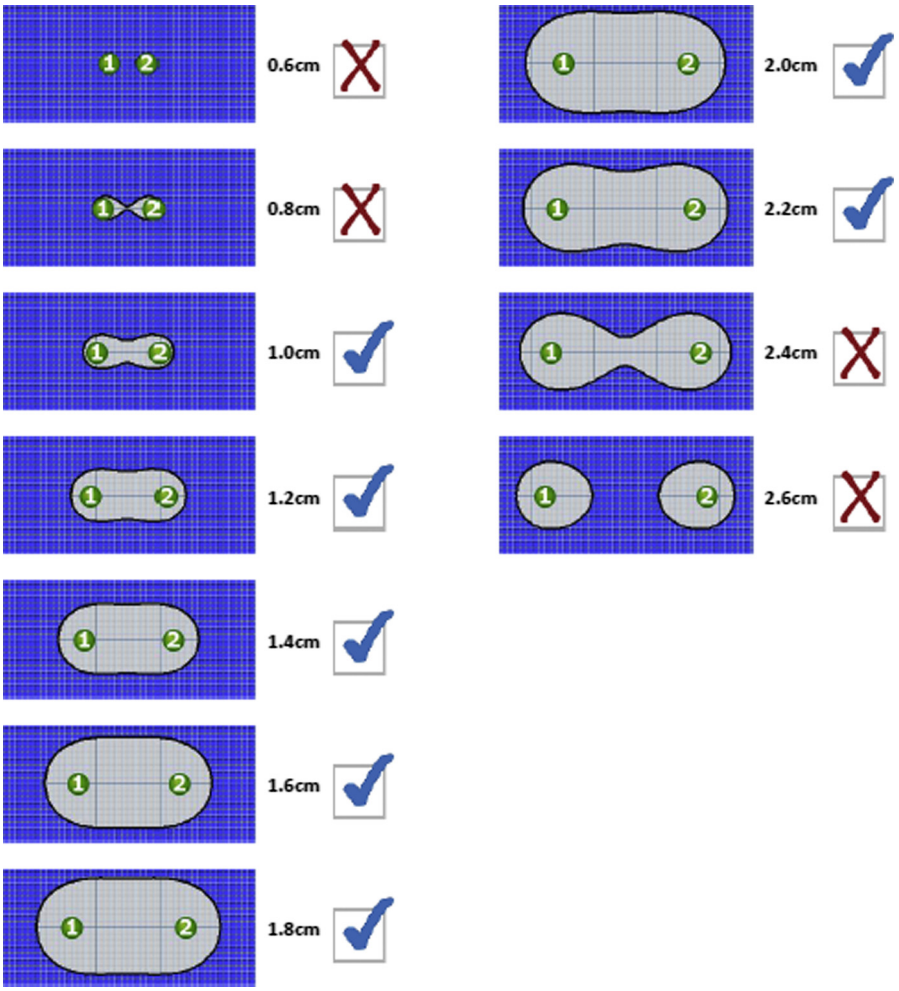

Fig 1. Expected regions of ablation. Check mark denotes where an apparent complete IRE would occur. X is where a skip or incomplete IRE would occur in the middle.

Ultrasonography. A BK FlexFocus 800 US machine with a continuous biplane probe/image was utilized for the entire needle placement during IRE delivery and for IRE evaluation after energy delivery. The maximum, axial, AP, and cranial-caudal images were obtained and measured.

Tissue Histology. After harvest, tissues were sectioned serially at 5-mm intervals, fixed in 10% neutral buffered formalin, and embedded in paraffin blocks. Histologic sections were cut and stained with hematoxylin and eosin for microscopic analysis.

Statistical evaluation. Actual and expected parameters of ablation (axial ablation, AP ablation, and volume) were correlated for each given probe spacing with respect to absolute difference. Expected ablation volumes were calculated using a cylindrical model as well as an ellipsoid model. A 2-sided *t* test was performed and *P* value calculated for each value or set of values for each given probe spacing. Correlation coefficient (r^2) was also calculated for the expected and actual values. Finally, dot plots were generated using Microsoft Excel and linear trendlines were drawn for each set of data to illustrate the relationship between actual and expected values.

RESULTS

A total of 20 ablations were performed on porcine liver/spleen with probe spacings ranging from 0.6 to 2.6 cm. With the exception of probe spacings of 0.6 and 0.8 cm, all other probe spacings were performed in duplicate. Expected dimensions and volumes of ablation as calculated using the AngioDynamics algorithm are shown in Table I. Visual representations of these theorized regions of ablation are shown in Fig 1. Actual dimensions and volumes of ablation are shown in Table II. A comparison of the actual and theorized regions of ablation is shown in Fig 2.

Table II. Actual ablation dimensions

Probe exposure (min)	*Probe spacing (cm)*	*Actual axial ablation distance (cm)*	*Actual AP ablation distance (cm)*	*Actual craniocaudal ablation distance (cm)*	*Ablation volume (cm^3)*
1	0.6	1.47	0.77	1.00	0.59
1	0.8	1.70	0.72	1.20	0.77
1	1.0	2.25	1.22	1.70	2.44
1	1.0	2.27	1.23	1.60	2.34
1	1.2	2.29	1.25	1.80	2.70
1	1.2	2.32	1.26	1.70	2.60
1	1.4	2.52	1.19	1.80	2.83
1	1.4	2.49	1.15	1.90	2.85
1	1.6	3.72	1.80	2.00	7.01
1	1.6	3.70	1.79	2.00	6.94
1	1.8	3.99	1.51	2.00	6.31
1	1.8	4.01	1.52	2.00	6.38
1	2.0	4.04	1.48	2.10	6.57
1	2.0	4.07	1.46	2.10	6.53
1	2.2	4.32	2.43	2.10	11.54
1	2.2	4.35	2.44	2.10	11.11
1	2.4	4.55	1.86	2.00	8.86
1	2.4	4.52	1.87	2.00	8.85
1	2.6	4.62	2.37	1.90	10.89
1	2.6	4.60	2.36	1.90	10.80

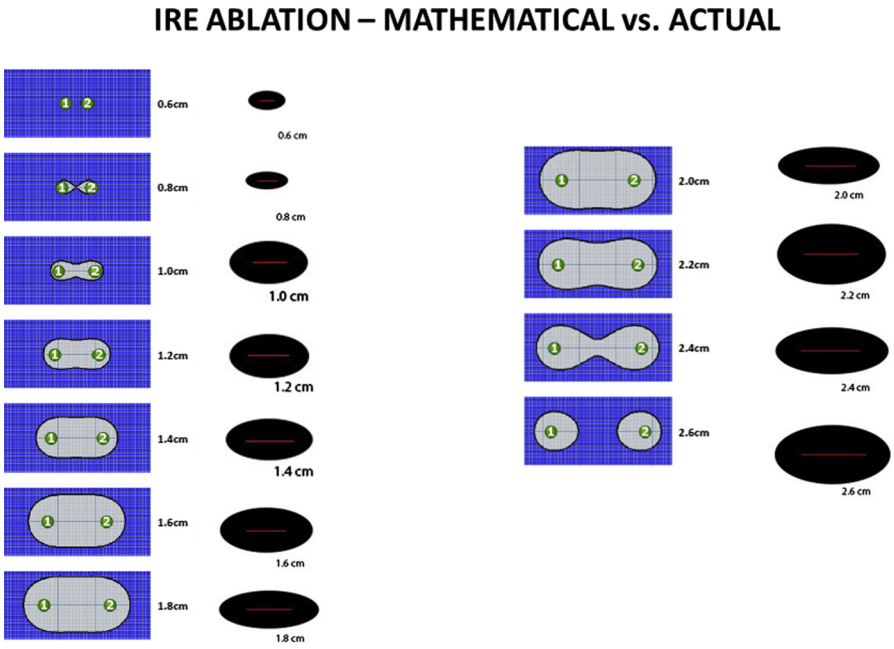

Fig 2. Mathematically estimated electroporation region (*left*) and actual in vivo irreversible electroporation (IRE) region (*right*).

When comparing the expected and actual dimensions of ablation (Table III), actual axial and AP dimensions were consistently greater than expected. Axially, all differences were statistically significant ($P \leq .05$). With respect to AP parameters, all differences were significant ($P \leq .05$) except those for probe spacing of 1.4 and 1.8 cm. Last, all craniocaudal distances were greater or equal to predicted values for probe spacings of 0.6, 0.8, 1.8, and 2.0 cm ($P \leq .05$). When calculating ablation volumes using a cylindrical model, actual ablation volumes were consistently greater than

Table III. Expected versus actual ablations

Probe spacing (cm)	*Expected vs actual axial ablation*	*Expected vs actual AP ablation distance*	*Expected vs actual craniocaudal ablation distance (cm)*	*Expected vs actual ablation volume*	*Expected vs actual ablation volume (ellipsoid)*
0.6	+1.27 ($P < .001$)	+0.57 ($P < .001$)	+0.20 ($P < .001$)	+0.584 ($P < .001$)	+0.573 ($P < .001$)
0.8	+0.901 ($P < .001$)	+0.32 ($P < .001$)	+0.20 ($P < .001$)	+0.669 ($P < .001$)	+0.602 ($P < .001$)
1.0	+0.850 ($P < .001$)	+0.92 ($P = .003$)	+0.1 ($P = .4265$)	+2.341 ($P = .0005$)	+2.089 ($P < .01$)
1.0	+0.870 ($P < .001$)	+0.93 ($P = .003$)	+0.0 ($P = .4265$)	+2.241 ($P = .0005$)	+2.079 ($P < .01$)
1.2	+0.490 ($P < .001$)	+0.35 ($P = .009$)	+0.20 ($P = .0955$)	+1.555 ($P = .0011$)	+1.297 ($P = .0015$)
1.2	+0.520 ($P < .001$)	+0.36 ($P = .009$)	+0.10 ($P = .0955$)	+1.455 ($P = .0011$)	+1.287 ($P = .0015$)
1.4	+.207 ($P = .05$)	+0.09 ($P = .177$)	+0.10 ($P = .0955$)	+0.644 ($P = .0002$)	+0.578 ($P = .0003$)
1.4	+.203 ($P = .05$)	+0.05 ($P = .177$)	+0.20 ($P = .0955$)	+0.664 ($P = .0002$)	+0.598 ($P = .0003$)
1.6	+1.00 ($P = .006$)	+0.40 ($P = .008$)	+0.10 ($P = .0960$)	+2.854 ($P = .0002$)	+3.234 ($P = .0001$)
1.6	+1.02 ($P = .006$)	+0.39 ($P = .008$)	+0.20 ($P = .0960$)	+2.784 ($P = .0002$)	+3.184 ($P = .0001$)
1.8	+1.09 ($P = .006$)	+0.01 ($P = .205$)	+0.20 ($P = .0122$)	+1.185 ($P = .0008$)	+1.987 ($P = .003$)
1.8	+1.11 ($P = .006$)	+0.02 ($P = .205$)	+0.25 ($P = .0122$)	+1.255 ($P = .0008$)	+2.047 ($P = .003$)
2.0	+0.85 ($P = .01$)	−0.12 ($P = .049$)	+0.10 ($P = .0423$)	+0.136 ($P = .0328$)	+1.208 ($P = .003$)
2.0	+0.85 ($P = .01$)	−0.14 ($P = .049$)	+0.15 ($P = .0423$)	+0.096 ($P = .0328$)	+1.168 ($P = .003$)
2.2	+1.02 ($P = .009$)	+1.03 ($P = .003$)	+0.10 ($P = .0955$)	+6.460 ($P = .0012$)	+6.636 ($P < .001$)
2.2	+1.05 ($P = .009$)	+1.04 ($P = .003$)	+0.20 ($P = .0955$)	+6.030 ($P = .0012$)	+6.706 ($P < .001$)
2.4	+1.15 ($P = .008$)	+0.66 ($P = .005$)	+0.15 ($P = .0377$)	+5.015 ($P < .0001$)	+4.806 ($P < .001$)
2.4	+1.12 ($P = .008$)	+0.67 ($P = .005$)	+0.10 ($P = .0377$)	+5.005 ($P < .0001$)	+4.786 ($P < .001$)
2.6	+1.02 ($P = .006$)	+1.27 ($P = .003$)	+0.20 ($P = .0122$)	+7.469 ($P < .0001$)	+7.320 ($P < .001$)
2.6	+1.00 ($P = .006$)	+1.26 ($P = .003$)	+0.20 ($P = .0122$)	+7.379 ($P < .0001$)	+7.320 ($P < .001$)
	$R^2 = 0.96$	$R^2 = 0.57$	$R^2 = 0.98$	$R^2 = 0.87$	$R^2 = 0.81$

expected ($P \leq .04$). Similarly, actual ablation volumes were consistently greater than those calculated using an ellipsoid model ($P \leq .01$).

The trends in expected and actual parameters of ablation are shown in Fig 3. Axial ablation distances with respect to probe spacing correlated well ($r^2 = 0.96$), as did the trend in expected and actual craniocaudal ablation distances ($r^2 = 0.98$) and expected and actual ablation volumes ($r^2 = 0.87$ for calculated cylindrical volumes, $r^2 = 0.81$ for calculated ellipsoid volumes). The correlation between expected and actual AP ablation distances with respect to probe spacing was less robust ($r^2 = 0.57$). Expected and actual axial distances seemed to increase relatively linearly and proportionally with respect to probe spacing. Although actual AP ablation distances demonstrated a fairly linear relationship, expected AP ablation distances displayed a more parabolic relationship, with a decrease in AP ablation distance of >2.0 cm probe spacing. Actual and expected craniocaudal ablation distances both displayed a parabolic relationship. Finally, actual ablation volumes demonstrated a relatively linear relationship with probe spacing, whereas expected ablation volumes based on both a cylindrical and an ellipsoid model exhibited a somewhat inverse cubic relationship.

DISCUSSION

In clinical practice, ablation planning using IRE depends on the use of mathematical models. These models derive from ex vivo data and theoretic tissue-specific conductivity. Since the emergence of IRE as an effective, nonthermal ablative technique for treatment of unresectable malignancies, multiple groups have analyzed the imaging and histologic characteristics of ablated tissue.[10,17,18,20-23] US, CT, and MRI have demonstrated good correlation with histopathologic findings.

Our data support findings suggested by other groups that the theorized dimensions and volumes of ablation correlate poorly with observed in vivo ablations. Actual ablation dimensions (AP, axial, craniocaudal) are greater than theorized. Although the relationships between axial ablation distances and craniocaudal distances for given probe spacings display a linear relationship and that for craniocaudal distances display a parabolic relationship for both the empiric and actual results, no such similarity exists for AP ablations. The linear relationship between probe spacing and distance of AP ablation observed with in vivo ablations fails to correlate with the parabolic observed in the theoretical model. This fact may result from the difference in geometry between the

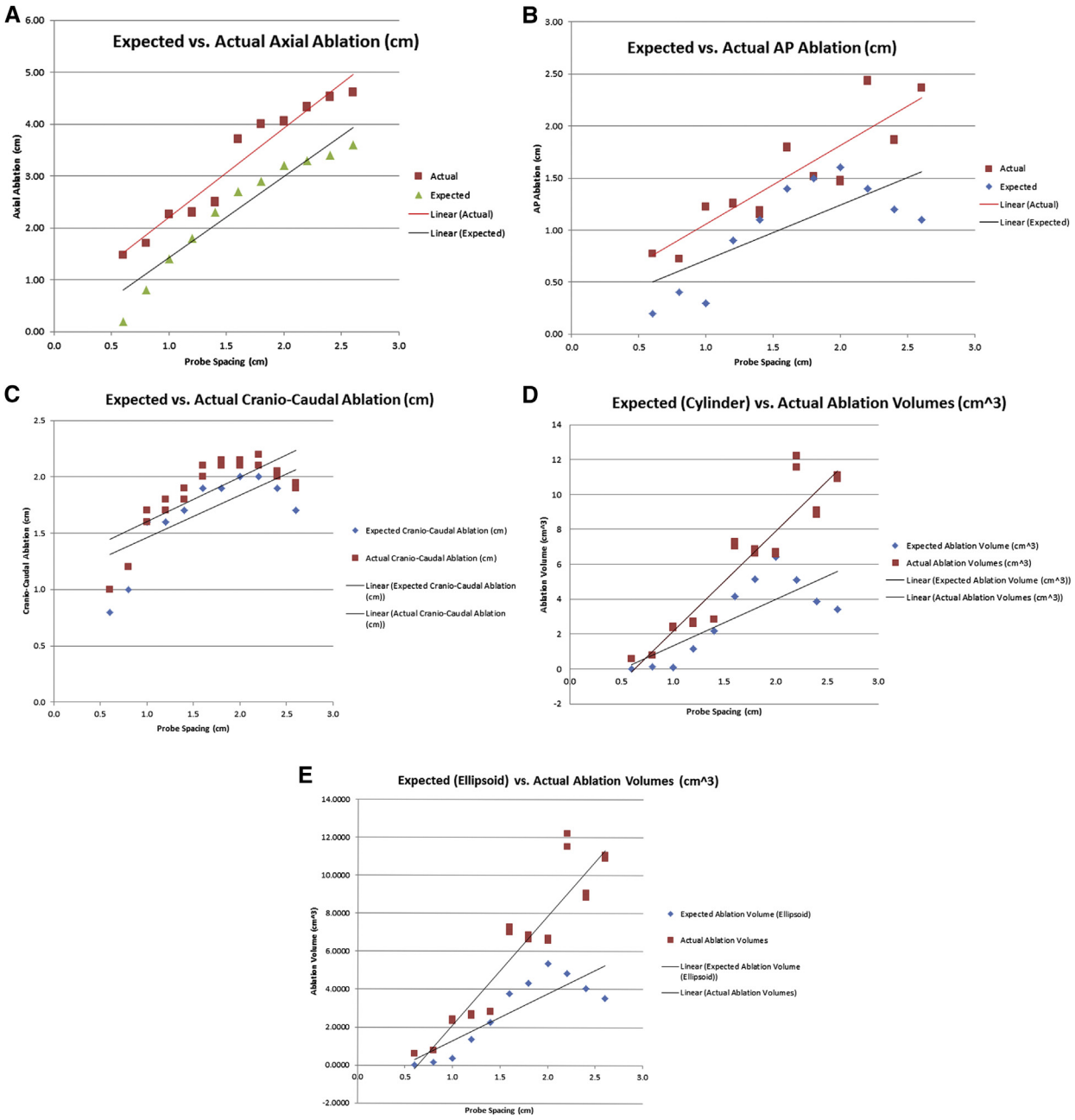

Fig 3. (*A*) Expected versus actual axial ablation. (*B*) Expected versus actual anterior-posterior (AP) ablation. (*C*) Expected versus actual craniocaudal ablation. (*D*) Expected (cylindrical) versus actual ablation volumes. (*E*) Expected (ellipsoid) versus actual ablation volumes.

expected and observed regions of ablation, which will be discussed in detail subsequently. Averaging multiple AP ablation diameters across the region would explain the progressively increasing discrepancy between expected and observed AP ablation distances at probe spacings of >2.0 cm. These findings confirm that the margin of error on IRE spacing is still narrow; however, these results do allow us to expect complete IRE confidently with spacing out to 2.6 cm. These results will not change the consistent message that our group has published previously but do allow us to have more definitive in vivo data.

Additionally, the geometry of ablated tissues varies. Specifically, modeled ablations demonstrate a progressively severe "necking" phenomenon with increasing probe distance of >2.0 cm. This effect is not observed in vivo, with the region between

probes displaying homogeneous, postablation echotexture on US with probe distance as great as 2.6 cm. This finding may result from different tissue conductivity than theorized or variable tissue conductivity at given distances from the electrodes as shown in previous studies.[24]

Finally, regarding ablated volumes, both with the cylindrical and ellipsoid models, the expected volumes were less than actual volumes. The implication of this geometric discrepancy would be that the volume not included in both the ellipsoid and cylindrical model would experience negligible or diminished ablation. This finding mirrors previously reported histologic findings of incomplete ablation effects near the periphery of projected ablation zones.[21]

Although our study demonstrates the discrepancy between hypothesized and actual regions of ablation, we have not determined how to improve modelling. Given the complexity of tissue microenvironments and overall tissue heterogeneity in vivo, producing an accurate mathematical model would prove both resource and time intensive. Such a tool would, however, prove invaluable in planning more accurately and effectively for tumor ablation, especially in proximity to important vascular structures.

In conclusion, our data show that theoretical models of IRE ablation misestimate ablation dimensions and volumes. In general, larger than intended cross-sectional areas experience ablative effects and areas at the periphery of cylinders centered around the probes may experience incomplete or no ablative effect at all. Physicians should consider carefully the limitations of mathematical models for IRE when planning ablations. This information highlights the limitations of current mathematical modeling and, by extension, our understanding of the exact mechanism of action of IRE. This information also emphasizes clearly that actual electrical potential differs from the model and thus can provide the potential IRE user a clear idea of what the "actual" IRE effect will be. This knowledge is essential to obtaining the highest quality of patient selection, IRE safety, and IRE efficacy. Serial imaging using US, CT, and/or MRI and histopathologic correlation can lead to the development of a superior model that will allow for more accurate ablative planning.

Dr Martin is a paid consultant for AngioDynamics. He provides physician training in the use of the NanoKnife irreversible electroporation system. Drs Bhutiani and Doughtie reported no biomedical financial interests or potential conflicts of interest.

REFERENCES

1. Ben-David E, Appelbaum L, Sosna J, Nissenbaum I, Goldberg SN. Characterization of irreversible electroporation ablation in in vivo porcine liver. AJR Am J Roentgenol 2012;198:W62-8.
2. Charpentier KP. Irreversible electroporation for the ablation of liver tumors: are we there yet? Arch Surg 2012;147:1053-61.
3. Deipolyi AR, Golberg A, Yarmush ML, Arellano RS, Oklu R. Irreversible electroporation: evolution of a laboratory technique in interventional oncology. Diagn Interv Radiol 2014;20:147-54.
4. Eller A, Schmid A, Schmidt J, et al. Local control of perivascular malignant liver lesions using percutaneous irreversible electroporation: initial experiences. Cardiovasc Intervent Radiol 2015;38:152-9.
5. Fritz S, Sommer CM, Vollherbst D, et al. Irreversible electroporation of the pancreas is feasible and safe in a porcine survival model. Pancreas 2015;44:791-8.
6. Janik V, Skrabalova D, Gurlich R, Malek J. [Irreversible electroporation: local, non-thermal, ablation therapy of malignant tumours]. Cas Lek Cesk 2013;152:67-75.
7. Rubinsky B, Onik G, Mikus P. Irreversible electroporation: a new ablation modality–clinical implications. Technol Cancer Res Treat 2007;6:37-48.
8. Scheffer HJ, Nielsen K, de Jong MC, et al. Irreversible electroporation for nonthermal tumor ablation in the clinical setting: a systematic review of safety and efficacy. J Vasc Interv Radiol 2014;25:997-1011. quiz.
9. Zhang Z, Li W, Procissi D, Tyler P, Omary RA, Larson AC. Rapid dramatic alterations to the tumor microstructure in pancreatic cancer following irreversible electroporation ablation. Nanomedicine (Lond) 2014;9:1181-92.
10. Hosein PJ, Echenique A, Loaiza-Bonilla A, et al. Percutaneous irreversible electroporation for the treatment of colorectal cancer liver metastases with a proposal for a new response evaluation system. J Vasc Interv Radiol 2014;25:1233-9.e2.
11. Sugimoto K, Moriyasu F, Kobayashi Y, Saito K, Takeuchi H, Ogawa S, et al. Irreversible electroporation for nonthermal tumor ablation in patients with hepatocellular carcinoma: initial clinical experience in Japan. Jpn J Radiol 2015;33:424-32.
12. Valerio M, Dickinson L, Ali A, et al. A prospective development study investigating focal irreversible electroporation in men with localised prostate cancer: Nanoknife Electroporation Ablation Trial (NEAT). Contemp Clin Trials 2014;39:57-65.
13. Valerio M, Stricker PD, Ahmed HU, Dickinson L, Ponsky L, Shnier R, et al. Initial assessment of safety and clinical feasibility of irreversible electroporation in the focal treatment of prostate cancer. Prostate Cancer Prostatic Dis 2014;17:343-7.
14. van den Bos W, de Bruin DM, Muller BG, et al. The safety and efficacy of irreversible electroporation for the ablation of prostate cancer: a multicentre prospective human in vivo pilot study protocol. BMJ Open 2014;4:e006382.
15. Pearson R, Lovewell, JG, Warden D, Morrison, DL, Sarno, TR, Lai, HT, et al. System and method for interactively planning and controlling a treatment of a patient with a medical treatment device. USA patent US20100249771 A1. 2010.
16. Au JT, Kingham TP, Jun K, et al. Irreversible electroporation ablation of the liver can be detected with ultrasound B-mode and elastography. Surgery 2013;153:787-93.
17. Wimmer T, Srimathveeravalli G, Gutta N, et al. Comparison of simulation-based treatment planning with imaging and

pathology outcomes for percutaneous CT-guided irreversible electroporation of the porcine pancreas: a pilot study. J Vasc Interv Radiol 2013;24:1709-18.
18. Zhang Y, White SB, Nicolai JR, et al. Multimodality imaging to assess immediate response to irreversible electroporation in a rat liver tumor model. Radiology 2014;271:721-9.
19. Appelbaum L, Ben-David E, Sosna J, Nissenbaum Y, Goldberg SN. US findings after irreversible electroporation ablation: radiologic-pathologic correlation. Radiology 2012; 262:117-25.
20. Lee YJ, Lu DS, Osuagwu F, Lassman C. Irreversible electroporation in porcine liver: acute computed tomography appearance of ablation zone with histopathologic correlation. J Comput Assist Tomogr 2013;37:154-8.
21. Wimmer T, Srimathveeravalli G, Gutta N, et al. Planning irreversible electroporation in the porcine kidney: are numerical simulations reliable for predicting empiric ablation outcomes? Cardiovasc Intervent Radiol 2015;38:182-90.
22. Lee YJ, Lu DS, Osuagwu F, Lassman C. Irreversible electroporation in porcine liver: short- and long-term effect on the hepatic veins and adjacent tissue by CT with pathological correlation. Invest Radiol 2012;47:671-5.
23. Schmidt CR, Shires P, Mootoo M. Real-time ultrasound imaging of irreversible electroporation in a porcine liver model adequately characterizes the zone of cellular necrosis. HPB (Oxford) 2012;14:98-102.
24. Ben-David E, Ahmed M, Faroja M, et al. Irreversible electroporation: treatment effect is susceptible to local environment and tissue properties. Radiology 2013;269:738-47.